Control of Hierarchical Order in Crystalline Composites of Diblock Copolymers and a Molecular Chromophore

Cara C. Evans, Frank S. Bates, and Michael D. Ward*

Department of Chemical Engineering and Materials Science, University of Minnesota, Amundson Hall, 421 Washington Avenue S. E., Minneapolis, Minnesota 55455

Received September 9, 1999. Revised Manuscript Received November 10, 1999

Addition of 2-chloro-4-nitroaniline (CNA) to diblock copolymers of poly(ethylene oxide) (PEO) and polystyrene (PS), poly(ethylethylene) (PEE), or poly(ethylenepropylene) (PEP) results in selective partitioning of CNA into the polar PEO domains. Calorimetry, infrared spectrosocpy, density measurements, and wide-angle X-ray diffraction support the formation of a crystalline molecular complex, comprising two ethylene oxide repeat units per one CNA. The structure of the complex is the same for PEO homopolymer and PEO-based diblocks. Wide-angle X-ray diffraction from uniaxially aligned samples of the PEO:CNA suggests a triclinic unit cell for the complex with $a = 9.08$ Å, $b = 10.48$ Å, $c = 7.01$ Å; and $\alpha = 90.98°$, $\beta = 88.38°$, and $\gamma = 116.72°$. The data are consistent with a structural model in which the PEO chains adopt a nominally all-trans zigzag configuration, the chains organized as (100) layers separated by layers of one-dimensional stacks of CNA molecules. Polarized infrared measurements indicate that the molecular planes of the CNA molecules are nominally perpendicular to the PEO chains. The metrics associated with the zigzag PEO configuration appear to allow for optimal hydrogen bonding between the PEO oxygen atoms and the amine protons of the CNA chromophores as well as hydrogen bonding between CNA molecules in adjacent stacks. The arrangement of the CNA molecules in the crystalline PEO:CNA complex differs from the structure of bulk CNA, clearly indicating that host−guest interactions play a major role in chromophore alignment. Small-angle X-ray scattering from a series of samples reveal changes in the block copolymer microstructure as the effective volume of the PEO block is altered by the inclusion of CNA. Whereas the SAXS data for PS-PEO and PEP−PEO copolymers used here reveal hexagonally packed cylinder microstructures in which cylinders of the minority PEO block are surrounded by PS or PEP, the lamellar microstructure is observed for all three block copolymers at the composition of the 2:1 complex. Consequently, these materials can be described as rigid crystalline molecular complexes embedded in robust, ordered polymer microstructures. This control of hierarchical order over length scales, spanning several orders of magnitude, suggests a route to permanent macroscopic ordering of functional molecules, a desirable feature for applications such as optoelectronics. The conformational rigidity associated with these systems offers considerable advantages for the design of SHG materials as entropically driven disordering is inhibited compared to noncrystalline polymer−chromophore materials.

Introduction

Polymers are commonly used as host matrices in a variety of functional composites in order to achieve properties or processing advantages that are not possible without the synergism between the host polymer and guest material. In this respect, a particularly ambitious goal has been the fabrication of composites, based on polymers and organic chromophores, for nonlinear optics applications.[1] In principle, organic chromophores can exhibit fast response times, be tailored through standard synthetic procedures, and readily converted into films by self-assembly,[2] Langmuir−Blodgett techniques[3] or, when included in polymer host matrices, cast from solution or the melt.[4]

The ability of polymer hosts to inhibit coalescence and control morphology has been illustrated by the preparation of metal,[5] metal oxide,[6] and semiconductor[7] nanoclusters in specific domains within functionalized polynorbornene block copolymers. Nanometer-scale platinum and palladium catalysts have been generated and stabilized within the polystyrene core of polystyrene-poly(ethylene oxide) (PS-PEO) block copolymer mi-

* To whom correspondence should be addressed. Phone: (612) 625-3062. Fax: (612) 626-7805. E-mail: wardx004@tc.umn.edu.

(1) *Special Polymers for Electronics and Optoelectronics*; Chilton, J. A., Goosey, M. T., Eds.; Chapman & Hall, London, 1995.

(2) See, for example: (a) Tew, G. N.; Li, L.; Stupp, S. I. *J. Am. Chem. Soc.* **1998**, *120*, 5601−5602. (b) Lenahan, K. M.; Wang, Y.-X.; Liu, Y. J.; Claus, R. O.; Heflin, J. R.; Marciu, D.; Figura, C. *Adv. Mater.* **1998**, *10*, 853−855. (c) Stupp, S. I.; LeBonheur, V.; Walker, K.; Li, L. S.; Huggins, K. E.; Keser, M.; Amstutz, A. *Science* **1997**, *276*, 384−389. (d) Lin, W.; Lee, T.-L.; Lyman, P. F.; Lee, J.; Bedzyk, M. J.; Marks, T. J. *J. Am. Chem. Soc.* **1997**, *119*, 2205−2211. (e) Lundquist, P. M.; Lin, W.; Zhou, H.; Hahn, D. N.; Yitzchaik, S.; Marks, T. J.; Wong, G. K. *Appl. Phys. Lett.* **1997**, *70*, 1941−1943. (f) Lin, W.; Lin, W.; Wong, G. K.; Marks, T. J. *J. Am. Chem. Soc.* **1996**, *118*, 8034−8042. (g) Roscoe, S. B.; Yitzchaik, S.; Kakkar, A. K.; Marks, T. J. *Langmuir* **1996**, *12*, 5338−5349.

10.1021/cm9905794 CCC: $19.00 © 2000 American Chemical Society
Published on Web 12/22/1999

celles.[8] Reverse micelles comprising these same blocks have been employed to stabilize gold nanoparticles.[9] These examples rely on particle growth and diffusion that is constrained by the domain size of the block containing the guest molecule. Microstructural templating of transition metal and inorganic materials has been demonstrated in a variety of diblock copolymers,[10] dendrimers,[11] lipids,[12] and liquid crystals.[13−15]

One of the greatest challenges in polymer-based optoelectronic materials has been the synthesis of materials with sustainable second-harmonic generation (SHG), a property that relies on the absence of centrosymmetry that accompanies anisotropic ordering of the molecular chromophores. While net polar orientation of organic chromophores dispersed in a polymeric film can be achieved by cooling a composite from the melt to the glassy state in the presence of an external electric field,[16] thermal reorganization of the chromophores commonly results in the decay of SHG efficiency.[4,17]

Scheme 1

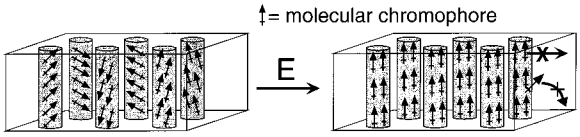

It is conceivable that the loss of anisotropic ordering can be suppressed by a strong interaction, such as hydrogen bonding, between the polymer and the chromophore. If the guest is confined within a specfic domain of a microstructured block copolymer due to immiscibility in the surrounding block component, the microstructure may further frustrate any reorientation of the chromophore, particularly if the host domain is crystalline and/or the surrounding block is glassy. Microphase separation in the copolymer can also produce microstructures capable of enforcing order of the chromophore-containing domains over a longer length scale. It may also be feasible to orient the domains of diblock copolymers by use of an appropriate substrate or application of an external electric field.[18] Consequently, the combination of hydrogen bonding and ordered microstructure formation may provide a hierarchical ordering over several orders of magnitude[19] that can lead to macroscopic ordering of the guest chromophore (Scheme 1).

An attractive block component for examining this hierarchical ordering is poly(ethylene oxide) (PEO), which is polar and can be integrated readily with nonpolar blocks to achieve microphase separation. Polar organic chromophores will tend to segregate into the polar PEO domains, while the hydrogen-bonding capacity of the PEO chain can enforce local ordering of guest chromophores containing hydrogen-bonding functionality. While molecular complexes in PEO have been reported, including both inorganic[20] and organic,[21−24] guests such as resorcinol[21a,c] or *p*-nitrophenol,[21a,b,25] complexes in copolymers have been limited.[26] Complexes

(3) See, for example: (a) Liu, S.-G.; Liu, Y.-Q.; Xu, Y.; Zhu, D.-B.; Yu, A.-C.; Zhao, X.-S. *Langmuir* **1998**, *14*, 690−695. (b) Ashwell, G. J.; Handa, T.; Jefferies, G.; Walker, T. W.; Bryce, M. R.; Grainger, A. M. *Supramol. Sci.* **1997**, *4*, 219−222. (c) Nguyen, D. M.; Mayer, T. M.; Hubbard, S. F.; Singer, K. D.; Mann, J. A., Jr.; Lando, J. B. *Macromolecules* **1997**, *30*, 6150−6157. (d) Xu, J.; Lu, X.; Kui, H.; Guangpeng, Z.; Zhang, Z. *Langmuir* **1997**, *13*, 3187−3190. (e) Ou, S. H.; Percec, V.; Mann, J. A.; Lando, J. B. *Langmuir* **1994**, *10*, 905−911. (f) Ashwell, G. J.; Jackson, P. D.; Crossland, W. A. *Nature* **1994**, *368*, 438−440. (g) Penner, T. L.; Motschmann, G. R.; Armstrong, N. J.; Ezenyilimba, M. C.; Williams, D. J. *Nature* **1994**, *367*, 49−51.

(4) See, for example: (a) Tirelli, N.; Suter, U. W.; Altomare, A.; Solaro, R.; Ciardelli, F.; Follonier, S.; Bosshard, Ch.; Günter, P. *Macromol.* **1998**, *31*, 2152−2159. (b) Mortaxavi, M.; Knoeson, A.; Kowel, S. T.; Higgins, B. G.; Diennes, A. *J. Opt. Soc. Am. B* **1989**, *6*, 733−741. (c) Singer, K. D.; Sohn, J. E.; Lalama, S. J. *Appl. Phys. Lett.* **1986**, *49*, 248−250. (d) Yitzchaik, S.; Berkovic, G.; Krongauz, V. *Chem. Mater.* **1990**, *2*, 162−168. (e) Meredith, G. R.; VanDusen, J. G.; Williams, D. J. *Macromolecules* **1982**, *15*, 1385−1389.

(5) (a) Yue, J.; Sankaran, V.; Cohen, R. E.; Schrock, R. R. *J. Am. Chem. Soc.* **1993**, *115*, 4409−4410. (b) Ng Cheong Chan, Y.; Craig, G. S. W.; Schrock, R. R.; Cohen, R. E. *Chem. Mater.* **1992**, *4*, 885−894.

(6) Sohn, B. H.; Cohen, R. E. *Chem. Mater.* **1997**, *9*, 264−269.

(7) (a) Fogg, D. E.; Radzilowski, L. H.; Dabbousi, B. O.; Schrock, R. R.; Thomas, E. L.; Bawendi, M. G. *Macromolecules* **1997**, *30*, 8433−8439. (b) Fogg, D. E.; Radzilowski, L. H.; Blanski, R.; Schrock, R. R.; Thomas, E. L. *Macromolecules* **1997**, *30*, 417−426. (c) Kane, R. S.; Cohen, R. E.; Silbey, R. *Chem. Mater.* **1996**, *8*, 1919−1924. (d) Lin, B. H.; Morkved, T. L.; Meron, M.; Huang, Z. Q.; Viccaro, P. J.; Jaeger, H. M.; Williams, S. M.; Schlossman, M. L. *J. Appl. Phys.* **1999**, *85*, 3180−3184.

(8) (a) Mayer, A. B. R.; Mark, J. E.; Morris, R. E. *Polym. J.* **1998**, *30*, 197−205. (b) Mayer, A. B. R.; Mark, J. E. *Colloid Polym. Sci.* **1997**, *275*, 333−340.

(9) (a) Spatz, J. P.; Roescher, A.; Möller, M. *Adv. Mater.* **1996**, *8*, 337−340. (b) Möller, M.; Spatz, J. P.; Roescher, A. *Macromol. Symp.* **1997**, *117*, 207−218.

(10) (a) Melosh, N. A.; Lipic, P.; Bates, F. S.; Wudl, F.; Stucky, G. D.; Fredrickson, G. H.; Chmelka, B. F. *Macromolecules* **1999**, *32*, 4332−4342. (b) De Paul, S. M.; Zwanziger, J. W.; Ulrich, R.; Wiesner, U.; Spiess, H. W. *J. Am. Chem. Soc.* **1999**, *121*, 5727−5736. (c) Templin, M.; Franck, A.; Du Chesne, A.; Leist, H.; Zhang, Y.; Ulrich, R.; Schadler, V.; Wiesner, U. *Science* **1997**, *278*, 1795−1798.

(11) Zhao, M.; Sun, L.; Crooks, R. M. *J. Am. Chem. Soc.* **1998**, *120*, 4877−4878.

(12) Puvvada, S.; Baral, S.; Chow, G. M.; Qadri, S. B.; Ratna, B. R. *J. Am. Chem. Soc.* **1994**, *116*, 2135−2136.

(13) Braun, P. V.; Osenar, P.; Stupp, S. I. *Nature* **1996**, *380*, 325−328.

(14) Gray, D. H.; Gin, D. L. *Chem. Mater.* **1998**, *10*, 1827−1832.

(15) Antonelli, D. M.; Ying, J. Y. *Curr. Opin. Colloid Interface Sci.* **1996**, *1*, 523−529 and references therein.

(16) (a) Goodwin, M. J.; Edge, G.; Trundle, C.; Bennion, I. *J. Opt. Soc. Am.* **1988**, *B5*, 419. (b) Singer, K. D.; Sohn, J. E.; Lalama, S. J. *Appl. Phys. Lett.* **1986**, *49*, 248. (c) Kobayashi, T.; Ohtani, H.; Kurokawa, K. *Chem. Phys. Lett.* **1985**, *121*, 336. (d) Chapoy, L. L.; Sethi, R. K.; Raun. P.; Rasmussen, K. H. *Polym. Photochem.* **1981**, *1*, 131. (e) Glen, R.; Goodwin, M. J.; Trundle, C. J. *Mol. Elec.* **1987**, *3*, 59. (f) Small, R. D.; Singer, K. D.; Sohn, J. E.; et al. *SPIE Proc.* **1986**, *682*, 160. (g) Esselin, S.; et al. *SPIE Proc.* **1988**, *971*, 120. (h) Khanarian, G. et al. *SPIE Proc.* **1987**, *682*, 153.

(17) (a) Hampsch, H. L.; Torkelson, J. M.; Bethke, S. J.; Grubb, S. G. *J. Appl. Phys.* **1990**, *67*, 1037−1041. (b) Hampsch, H. L.; Yang, J.; Wong, G. K.; Torkelson, J. M. *Macromolecules* **1990**, *23*, 3640−3647. (c) Hampsch, H. L.; Yang, J.; Wong, G. K.; Torkelson, J. M. *Macromolecules* **1990**, *23*, 3648−3654.

(18) (a) Amundson, K. R. *Plast. Eng.* **1998**, *45*, 1079−1139. (b) Morkved, T. L.; Lu, M.; Urbas, A. M.; Ehrichs, E.; Jaeger, H. M.; Mansky, P.; Russell, T. P. *Science* **1996**, *273*, 931−933. (c) Amundson, K.; Helfand, E.; Quan, X.; Hudson, S. D.; Smith, S. D. *Macromolecules* **1994**, *27*, 6559−6570. (d) Amundson, K.; Helfand, E.; Quan, X.; Smith, S. D. *Macromolecules* **1993**, *26*, 2698−2703. (e) Amundson, K.; Helfand, E.; Davis, D. D.; Quan, X.; Patel, S. S.; Smith, S. D. *Macromolecules* **1991**, *24*, 6546−6548.

(19) (a) Ruokolainen, J.; Torkkeli, M.; Tanner, J.; Serimaa, R.; tenBrinke, G. *Colloids Surf. A* **1999**, *147*, 241−248. (b) Ruokolainen, J.; Makinen, R.; Torkkeli, M.; Makela, T.; Serimaa, R.; tenBrinke, G. J.; Ikkala, O. *Science* **1998**, *280*, 557−560. (c) Dormidontova, E.; ten Brinke, G. *Colloids Surf. A* **1999**, *147*, 249−262. (d) Ruokolainen, J.; Saariaho, M.; Ikkala, O.; ten Brinke, G.; Thomas, E. L.; Torkkeli, M.; Serimaa, R. *Macromolecules* **1999**, *32*, 1152−1158.

(20) (a) Lemmon, J. P.; Lerner, M. M. *Chem. Mater.* **1994**, *6*, 207−210. (b) Lascaud, S.; Perrier, M.; Vallée, A.; Besner, S.; Prud'homme, J.; Armand, M. *Macromolecules* **1994**, *27*, 7469−7477. (c) Lightfoot, P.; Mehta, M. A.; Bruce, P. G. *Science* **1993**, *262*, 883−885. (d) Chatani, T.; Okamura, S. *Polymer* **1987**, *28*, 1815−1819. (e) Yokoyama, M.; Ishihara, H.; Iwamoto, R.; Tadokoro, H. *Macromolecules* **1969**, *2*, 184−192. (f) Iwamoto, R.; Saito, Y.; Ishihara, H.; Tadokoro, H. *J. Polym. Sci., A-2* **1968**, *6*, 1509−1525.

(21) (a) Spevácek, J.; Paternostre, L.; Damman, P.; Draye, A. C.; Dosière, M. *Macromolecules* **1998**, *31*, 3612−3616. (b) Damman, P.; Point, J. J. *Polym. Int.* **1995**, *36*, 117−125. (c) Delaite, E.; Point, J.-J.; Damman, P.; Dosière, M. *Macromolecules* **1992**, *25*, 4768−4778. (d) Point, J. J.; Damman, P. *Macromolecules* **1991**, *24*, 2019−2023. (e) Cheng, C.; Belfiore, L. A. *Polym. Prepr.* **1989**, *30*, 325−326.

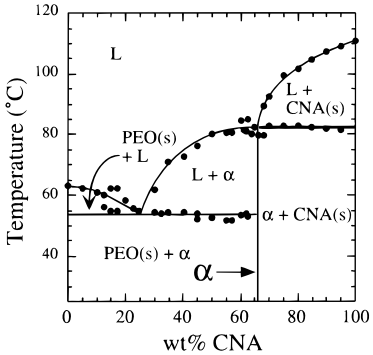

Figure 1. (a) Phase diagram constructed for PEO and CNA using differential scanning calorimetry and infrared spectroscopy. The lines represent estimates of the phase boundary regions.

of NaSCN and PEO have been reported for PEO-based block copolymers, but to our knowledge the effect on the microstructure of the diblock copolymer has not been definitively characterized.[27]

Herein we report that the addition of 2-chloro-4-nitroaniline (CNA), a chromophore with potential for nonlinear optics,[28] to PEO homopolymer and diblock copolymers of PEO and polystyrene (PS-PEO), poly(ethylethylene) (PEE-PEO), or poly(ethylenepropylene) (PEP-PEO) results in highly selective partitioning of CNA into the polar PEO domains. This segregation is driven by the formation of a crystalline hydrogen-bonded molecular complex that comprises two EO units per one CNA molecule in both the PEO homopolymer and the block copolymers. Although the pure copolymers possess hexagonally packed PEO cylinders surrounded by PS or PEP, selective partitioning of CNA affords a lamellar microstructure for the complex. These observations indicate that it is possible to confine organic chromophores within specific block copolymer domains through formation of rigid crystalline complexes while achieving microstructural order at longer length scales.

Results and Discussion

Solubility of CNA in PEO Homopolymer and Complex Formation. The phase diagram of CNA and PEO (Figure 1), determined by differential scanning calorimetry, reveals the existence of a eutectic point at 25 wt % CNA and 54 °C and the formation of a molecular complex (α). The phase diagram closely resembles that reported for *p*-nitrophenol in PEO.[21b]

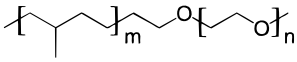

PEE-PEO

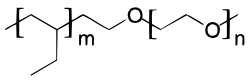

PEP-PEO

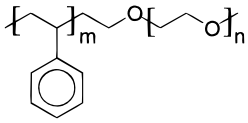

PS-PEO

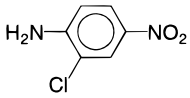

CNA

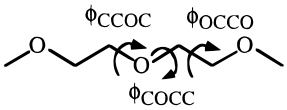

The stoichiometry of the CNA/PEO complex corresponds to one CNA molecule per two EO units (66.2 wt % CNA), determined by locating the cusp in the plot of the total enthalpy of fusion. The presence of this complex and its stoichiometry were corroborated by infrared spectroscopy, in which the complex was signified by a 16 cm^{-1} red shift of the symmetric $\nu_s(NH_2)$ mode of CNA, relative to CNA in Nujol (Figure 2). This indicates that hydrogen bonding of CNA to PEO in the complex is stronger than the intermolecular hydrogen bonding in pure CNA crystals. At CNA concentrations equal to or exceeding 66.2 wt % the asymmetric $\nu_s(NH_2)$ mode of bulk CNA appears as a doublet at 3494/3474 cm^{-1} that can be attributed to the pure chromophore. These same bands are observed at 3525 and 3420 cm^{-1} in saturated hexane solutions where intermolecular hydrogen bonding is nominally absent.

Wide-angle X-ray scattering (WAXS) patterns of uniaxially drawn films of samples having the 2:1 PEO:CNA composition revealed well-defined diffraction patterns associated with crystalline ordering. The data obtained with a 2-D area detector for numerous samples were essentially identical, although variable in quality and the extent of residual uncomplexed crystalline PEO.[29] The data presented in Figure 3 represent the highest degree of alignment and best resolved reflections among the samples examined, although it also exhibits several reflections from residual PEO. (It was later discovered that the residual PEO reflections could be eliminated entirely by soaking fibers of α in ether solutions saturated with CNA.)

The reflections remaining after subtracting the reflections from uncomplexed PEO cannot be assigned to CNA[30] alone, indicating that α is crystalline. Assigning

(22) (a) Point, J. J.; Demaret, J. Ph. *J. Phys. Chem.* **1987**, *91*, 797–799. (b) Point, J. J.; Coutelier, C.; Villers, D. *J. Phys. Chem.* **1986**, *90*, 3277–3282. (c) Point, J. J.; Jasse, B.; Dosiere, M. *J. Phys. Chem.* **1986**, *90*, 3273–3277.

(23) Watanabe, T.; et al. *Mater. Res. Soc. Symp. Proc.* **1988**, *109*, 339.

(24) Kono, K.; Tekeda, Y.; Nogami, H.; Nagai, T. *Chem. Pharm. Bull.* **1974**, *22*, 165–170.

(25) (a) Damman, P.; Point, J. J. *Macromolecules* **1995**, *28*, 2050–2053. (b) Damman, P.; Point, J. J. *Macromolecules* **1994**, *27*, 3919–3925. (c) Damman, P.; Point, J. J. *Macromolecules* **1993**, *26*, 1722–1728. (d) Point, J. J.; Damman, P. *Macromolecules* **1992**, *25*, 1184–1188.

(26) Goldacker, T.; Abetz, V.; Stadler, R.; Erukhimovich, I.; Leibler, L. *Nature* **1999**, *398*, 137.

(27) (a) Robitaille, C.; Prud'homme, J. *Macromolecules* **1983**, *16*, 665. (b) Eastmond, G. C.; Schofield, P.; Sakellariou, P. *Polymer* **1997**, *38*, 1753–1761.

(28) Levine, B. F.; Bethea, C. G.; Thurmond, C. D.; Lynch, R. T.; Bernstein, J. L. *J. Appl. Phys.* **1979**, *50*, 2523–2527.

(29) Takahashi, Y.; Tadokoro, H. *Macromolecules* **1973**, *6*, 672.

(30) McPhail, A. T.; Sim, G. A. *J. Chem. Soc.* **1965**, 227.

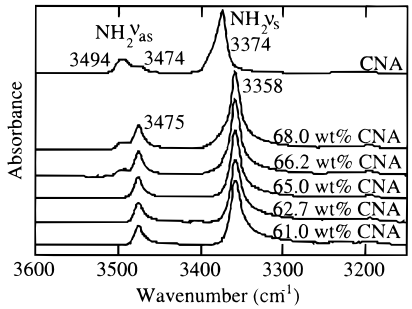

Figure 2. Infrared spectra for CNA in Nujol and PEO. The bands can be attributed to the asymmetric and symmetric stretch of the amine substituent.

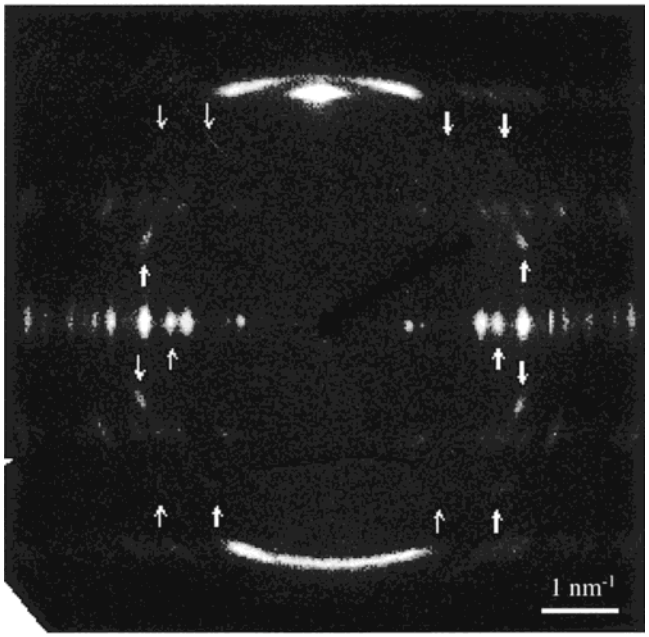

Figure 3. WAXS pattern acquired with a 2D area detector acquired for a uniaxially aligned fiber of the PEO-CNA molecular complex α (66.2 wt % CNA). The fiber axis was oriented vertically with respect to the pattern. Reflections from residual PEO are indicated by arrows.

the fiber axis to [001], c^* was calculated from the positions of the meridional reflections. The best fit to experimental data was a triclinic cell with $a = 9.08$, $b = 10.48$, $c = 7.01$ Å, $\alpha = 90.98$, $\beta = 88.38$, $\gamma = 116.72°$ (see Experimental Section and Supporting Information for details) The space group can be assigned as $P1$ (noncentrosymmetric) or $P\bar{1}$ (centrosymmetric), the data not allowing an unambiguous choice among these two space groups.

The density of the complex, measured by the flotation method, was 1.40 g/cm^3, comparable to the value of 1.45 g/cm^3 calculated for four EO units and two CNA molecules, and corresponding to the 2:1 stoichiometry of α in a unit cell having the volume determined from the X-ray data ($V = 596$ Å^3). Assuming that the polymer chains of the fiber are oriented along [001], and that the unit cell contains two polymer chains projected on the (001) plane, each polymer chain will have two ethylene oxide repeat units in the fiber period of 7.01 Å. This dimension is slightly less than the fiber period reported for two EO repeat units in the planar zigzag conformation of PEO under tension (7.12 Å),[31] suggesting that the polymer backbone of the molecular complex is described by a planar zigzag conformation with all, or nearly all, trans configurations. In contrast, pure PEO adopts a 7_2 helical conformation with repeating trans, trans, and gauche conformations, associated with dihedral angles ϕ_{CCOC}, ϕ_{COCC}, and ϕ_{OCCO}.[29]

To further characterize the structure of α, the mid- and far-infrared spectra of the complex in PEO and in perdeuterated PEO were compared with that obtained for CNA and PEO (see Table 4). Although many vibrational modes in the spectrum of the molecular complex can be reliably assigned, some assignments are ambiguous because (i) the shift of bands from the positions for pure starting materials cannot be precisely predicted, (ii) the bands from PEO and CNA may overlap, and (iii) a particular band observed in both PEO and deuterated PEO may be due to a polymer backbone vibrational mode of PEO that is a consequence of complex formation, so this band cannot be assumed to be due to CNA in the complex. This ambiguity can be illustrated by the appearance of bands at 1319 and 1127 cm^{-1} in the complex. The possibility that these bands could be attributed to modes of the chromophore (ν_{CN} and β_{CH}, respectively) precludes their respective assignment as solely $\delta(CH_2)$ of trans $O-(CH_2)_2-O$[20f,32] and ν_{COC} of PEO.

Nevertheless, the spectra support the presence of a zigzag PEO chain for the complex rather than a helical conformer. Rocking modes of the methylene groups of pure PEO absorb at 958 (∥), 947 (⊥), and 844 (⊥) cm^{-1}. The molecular complex, on the other hand, exhibits only a singlet at 959 (⊥) cm^{-1} and a peak at 837 (∥) cm^{-1}, the latter possibly due to CNA. Similarly, fewer bands attributable to bending, wagging, and twisting modes of the polymer methylene groups were observed for the complex relative to the spectrum of the pure polymer. This reduction of the number of bands has been reported to signify the presence of a planar zigzag conformation in blends of PEO and PMMA.[33,34] The locations of the unambiguously assigned PEO modes for PEO-PMMA blends and α are identical to within 10 cm^{-1}.

The spectrum of α also resembles that of the type I PEO:$HgCl_2$ complex, in which every other dihedral angle about $O-(CH_2)_2-O$ is 180°.[20f] The PEO:CNA and PEO:$HgCl_2$ complexes both exhibit a band at ~1015 cm^{-1} that can be attributed to $r(CH_2)_a + \nu(COC)$ of trans $O-(CH_2)_2-O$.[20f,32] In contrast, there are few similarities between the infrared spectroscopic data for α and PEO complexed with para-dihalogenated benzene compounds. In these complexes PEO adopts a helical conformation for which the A_2 doublet of the $\delta(OCC)_a$ mode of the pure polymer (529, 510 cm^{-1}) simply shifts to 523 and 515 cm^{-1} while the E_1 band remains at 534 cm^{-1}.[22c] The PEO-CNA complex, however, exhibits no bands between 500 and 530 cm^{-1}, and the band remaining at 534 cm^{-1} may be due to a CNA mode.[35]

(31) Takahashi, Y.; Sumita, I.; Tadokoro, H. *J. Polym. Sci.* **1973**, *11*, 2113−2122.
(32) Jeevanandam, P.; Vasudevan, S. *Chem. Mater.* **1998**, *10*, 1276−1285.
(33) Marcos, J. I.; Orlandi, E.; Zerbi, G. *Polymer* **1990**, *31*, 1899−1903.
(34) Rao, G. R.; Castiglioni, C.; Gussoni, M.; Zerbi, G.; Martuscelli, E. *Polymer* **1985**, *26*, 811−820.
(35) Varsanyi, G. *Assignments for Vibrational Spectra of Seven Hundred Benzene Derivatives*; John Wiley & Sons: New York, 1974; Vol. 1.

The existence of a near zigzag conformation in α instead of the 7_2 helix observed for pure PEO is not unreasonable as the calculated energy of the planar zigzag conformer is lower than that of the 7_2 helix by only 0.1 kcal/mol monomer unit.[36] Furthermore, as noted above, a variety of skeletal dihedral angles for the trans, trans, gauche sequence of the 7_2 helix have been reported for other complexes with PEO, indicating that the skeletal conformation is rather soft and deformable in the presence of PEO−guest interactions. Indeed, the splitting of the PEO band at 2886 cm^{-1} into two bands at 2914 and 2873 cm^{-1},[37] observed here for α, has been described as a signature of strong PEO-guest interactions in other materials.[38−40]

While the infrared data for the PEO-CNA complex suggests a zigzag conformation, it is important to note that the measured spectra differ somewhat from that reported previously for all-trans PEO, formed under tension.[31] The bands that have tentatively been assigned to PEO in α are consistently blue shifted relative to the planar zigzag conformer, the magnitude of the shift being greater for methylene group modes than for skeletal vibrations of the polymer backbone. These blue shifts suggest a "stiffening" of the local methylene vibrational modes due to interaction of PEO with CNA and differences in the packing of the PEO chains. The slightly smaller *c* lattice constant for α (only 1.5% smaller than the fiber repeat period for pure planar zigzag PEO) also suggests slight conformational differences ($\phi \neq 180°$), which can influence the local vibrational modes.

In addition to the red shifts of $\nu_{as}(NH_2)$ and $\nu_s(NH_2)$ described above for CNA, the infrared data reveal shifts of bands in α assigned to $\beta_s(NH_2)$, $\nu(CN)$, $\beta_{as}(NH_2)$, and $\beta_s(NO_2)$. The dichroic behaviors of these and other modes were examined to characterize the orientation of the chromophore with respect to the fiber axis. Spectra of a uniaxially aligned film of the complex in PEO were recorded with light polarized 0° ($A_{||}$) or 90° ($A_{\perp}$) with respect to the fiber axis (Table S1). Normal modes of CNA, which belongs to point group C_s, are classified by a change in dipole moment that is perpendicular (a′) or parallel (a″) to the plane of the phenyl ring. The few out-of-plane vibrations that can be assigned to CNA in α are polarized parallel to the fiber axis. In contrast, perpendicular polarization is exhibited by in-plane modes, which include ring stretches as well as vibrations involving the amine or nitro substituents. The infrared data indicate that the molecular plane of CNA in α is nominally perpendicular to the fiber axis.

The X-ray, calorimetric, and infrared data combined allow construction of a structural model of the PEO-CNA molecular complex (Figure 4). The two polymer chains of the basis, as projected on the (001) plane, were placed at (0,0) and (0.5,0). The resulting distance between the nearest neighbor polymer chains, 4.45 Å, is close to the values reported for both planar zigzag PEO under tension[31] and PEO in other molecular complexes.[20f,22b] The polymer chains were rotated about the fiber axis until optimal space-filling was achieved, followed by placing CNA molecules in the unit cell so that the phenyl rings were parallel to (001) and, hence, nominally perpendicular to the fiber axis. The precise azimuthal orientation of CNA in the (001) plane or the mutual orientations of the CNA dipoles could not be determined from our data. However, modeling studies revealed that the *b* lattice parameter is too small to allow orientation of the CNA dipolar axis along *b*. This precludes an orientation with both amine hydrogen atoms interacting with a single ether oxygen in an EO segment. Consequently, the model was constructed with each CNA molecule oriented so that only *one* amine hydrogen per CNA was directed toward the ether oxygen in a given EO segment. This structure affords (CNA)N−H···O(PEO) distances of 2.9 Å, which would signify rather weak hydrogen bonds.[41] However, the model suggests (CNA)C−H···O(PEO) hydrogen bonds which, although generally weak, may serve an important role in stabilizing the complex. Weak hydrogen bonding along *a* between the other amine hydrogen and a (nitro)oxygen atom of an adjacent CNA molecule, with (CNA)N−H···O−N(CNA) distances of 2.4 Å, is also revealed.

The relatively large hydrogen-bonding distances suggest that the CNA-PEO and CNA-CNA hydrogen-bonding interactions are weak. This contradicts the infrared spectroscopic data, which suggest instead that the hydrogen bonding of CNA in the complex is stronger than in pure CNA (vide ante). This apparent contradiction reflects the inherent imprecision of a model in which the positions and orientations of the CNA molecules are not exactly known. While it is difficult to rank the importance of host−guest and guest−guest hydrogen bonding and van der Waals interactions with respect to their influence on structure determination, it is evident that the arrangement of the CNA molecules in the crystalline PEO:CNA complex differs from the structure of bulk CNA, indicating that host−guest interactions play a major role in CNA alignment.

The fiber repeat distance, $c = 7.01$ Å, suggests a separation of 3.50 Å between the mean planes of the CNA phenyl rings. This separation is identical to the interplanar separation between CNA molecules in crystalline CNA,[30] in which CNA molecules, with their dipolar axes parallel, are assembled into stacks directed by Cl−Cl interactions[42] (Figure 4c). The model of α in Figure 4 is depicted with CNA molecules oriented antiparallel within each stack, a configuration expected to be favored by dipole−dipole energies. This configuration also allows hydrogen bonding interactions be-

(36) Tai, K.; Tadokoro, H. *Macromolecules* **1974**, *7*, 507−515.

(37) The spectra of the polyethylene substrates used to collect some of the data in Table 4 did have bands at 2918 (medium intensity) and 2874 (very weak) cm^{-1}. However, bands at these approximate frequencies in the spectra of the complex were not simply from polyethylene, since they also appeared in the spectra of films cast on NaCl and of free-standing films.

(38) Aranda, P.; Ruiz-Hitzky, E. *Chem. Mater.* **1992**, *4*, 1395−1403.

(39) Nazar, L. F.; Wu, H.; Power, W. P. *J. Mater. Chem.* **1995**, *5*, 1985−1993.

(40) Jeevanandam, P.; Vasudevan, S. *Chem. Mater.* **1998**, *10*, 1276−1285.

(41) Typical distances between H and O for N−H···O hydrogen bonds are between 1.60 and 2.40 Å (Bernstein, J.; Etter, M. C.; Leiserowitz, L. In *Structure Correlation*, Bürgi, H.-B., Dunitz, J. D., Eds.; VCH Publishers: New York, 1994; Vol. 2, p 433). The lengths cited for the hydrogen bonds with the ether oxygens of the polymer chain are rather long; the actual distances may be shorter. The exact position of the CNA molecules with respect to the polymer chains cannot be determined from the present data.

(42) Desiraju, G. R. *Organic Solid State Chemistry*; Elsevier: New York, 1987; Vol 32.

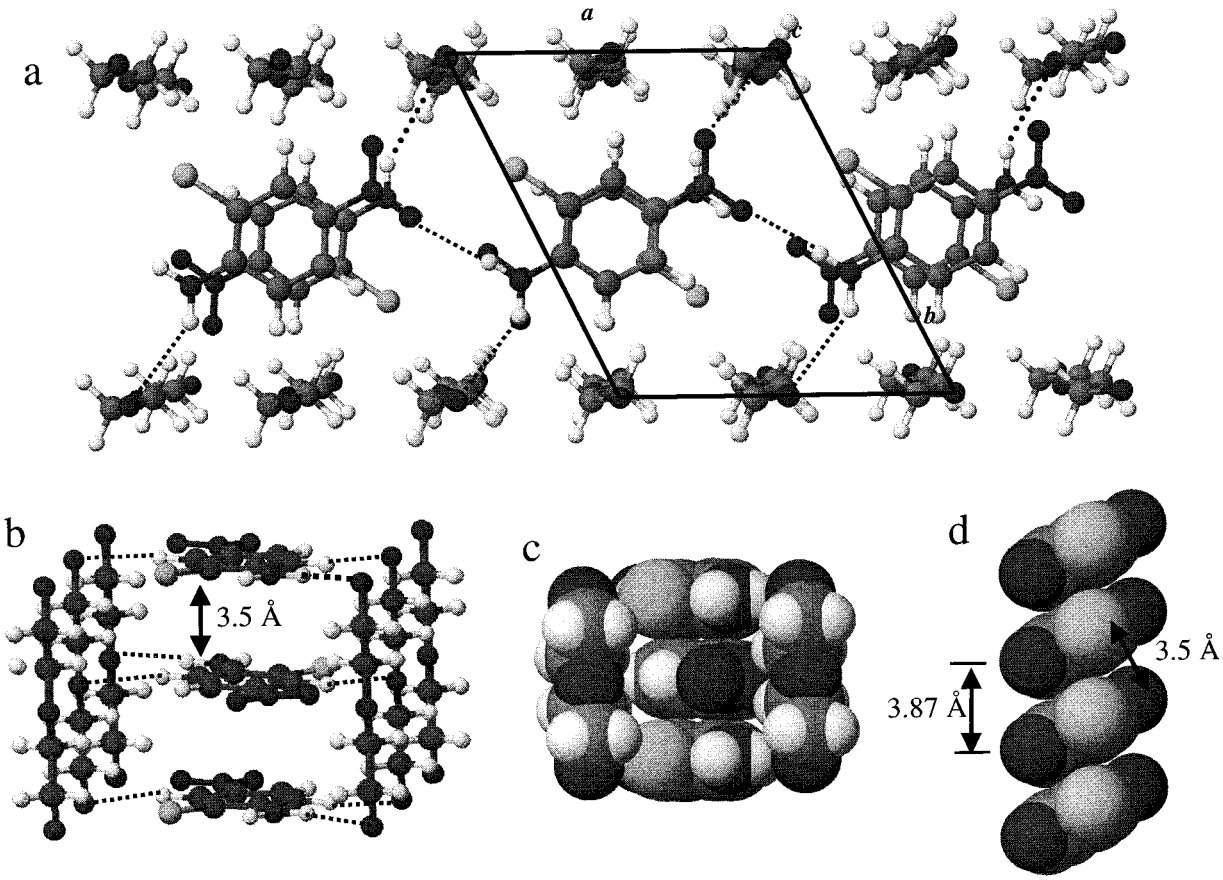

Figure 4. (a) View along [001] of the P$\bar{1}$ model structure for the PEO:CNA complex α, with $a = 9.08$, $b = 10.48$, $c = 7.01$ Å; and $\alpha = 90.98$, $\beta = 88.38$, and $\gamma = 116.72°$. The PEO chain is depicted with the same conformation (all-trans zigzag) and fiber period (7.12 Å) as that published previously.[29,31] The molecular structure of CNA was obtained from the single-crystal structure of pure CNA,[30] with hydrogen atoms added in idealized positions. The (CNA)N—H···O(PEO) hydrogen bonds in the CNA (001) layers are indicated by dashed lines. The mutual orientation of CNA molecules within a given stack is depicted here as antiparallel, which would maximize dipole–dipole interactions as well as optimize PEO-CNA hydrogen bonding. However, there is no evidence that argues against a noncentrosymmetric alternative in which the dipoles are parallel. (b) View of the model structure roughly perpendicular to ⟨001⟩. The (CNA)N—H···O(PEO) and (CNA)C— H···O(PEO) hydrogen bonding is indicated by the dashed lines. (c) View of the model structure perpendicular to ⟨001⟩ as a space filling representation. (d) The stacking motif existing in pure CNA.[30] While the *c* lattice parameter is 3.87 Å, the mean planes of the phenyl rings are not perpendicular to ⟨001⟩ and are 3.5 Å apart.

tween the PEO oxygen and CNA amine hydrogen atoms. However, the well-documented structure-directing influence of Cl—Cl interactions[42] cannot be ignored. A parallel alignment of CNA dipoles within each stack that mimicks the bulk structure is also feasible. The antiparallel and parallel configurations would correspond to the centrosymmetric $P\bar{1}$ and noncentrosymmetric $P1$ structures, respectively, which, as stated above, cannot be distinguished by the X-ray data.

It should also be noted that the model of α differs from pure CNA with respect to the angle between the molecular planes and the stacking axis, which can be attributed to different packing constraints in the two materials. The shorter *c* lattice constant in α rules out the tilting of the molecular planes that exists in pure CNA.

Host–Guest Complex Formation in Diblock Copolymer PEO Domains. Like the complex in homopolymeric PEO, the presence of the PEO:CNA molecular complex α in the diblock copolymers was evident from infrared spectroscopic and wide-angle X-ray diffraction data. The bands at 3475 and 3358 cm^{-1} that are characteristic of α were observed in spectra of aged samples containing 66.2 wt % CNA *relative to PEO*, in PS-PEO, PEE-PEO, or PEP-PEO (Figure 5, Table 1). These bands required days to develop, and did so at variable and irreproducible rates. This suggests that relative to complex formation in the PEO homopolymer, the formation of the molecular complex in the PEO domains of the diblock copolymer was kinetically inhibited.

The most likely explanation for this phenomenon is hampered diffusion of the PEO chains, imparted by the nonpolar blocks, that would frustrate the conformational changes and reorganization required to form the complex. Previous studies of PEO-based block copolymers containing complexes NaSCN in the PEO domains attributed lower crystallization temperatures to the existence of finely dispersed microdomains of the crystallizable component, which frustrates nucleation throughout the PEO domain.[27a] Notably, samples prepared at the 2:1 composition of α displayed neither a band at 3376 cm^{-1}, corresponding to precipitated CNA in either block, nor bands that would signify CNA dissolved in the nonpolar block. This observation is consistent with selective incorporation of CNA in the PEO domains at and below the composition of the complex.

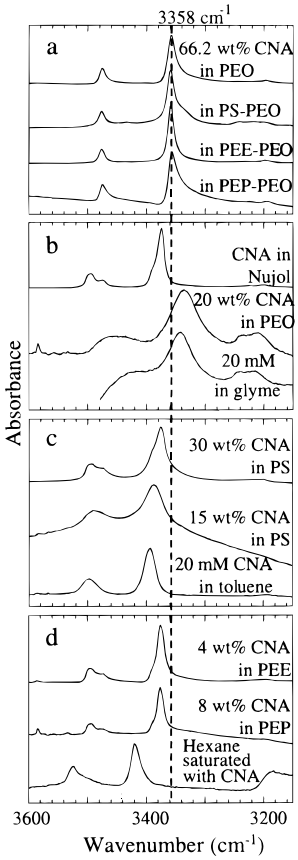

Figure 5. Infrared spectra of the NH_2 stretching region for CNA in various media at room temperature. The weak band at 3475 and the strong band at 3358 cm^{-1} are characteristic of the molecular complex α. (a) The PEO-CNA molecular complex in PEO and in the PEO block of three diblock copolymers. In each matrix, the concentration of CNA was 66.2 wt % with respect to PEO (2:1 EO units per CNA). (b, c, and d) Comparison of the infrared spectra of CNA in various polymers and solvents. CNA dissolves readily in PEO, and somewhat in PS, but precipitates in PEE or PEP.

Table 1. Selected Properties of the Polymers Examined

polymer	molecular weight ($\times 10^3$ g/mol)	f_{PEO}[a]	composition (wt % CNA[b] with respect to PEO[c])	$f_{(PEO+CNA)}$[a]
PS-PEO	31	0.22	66.2	0.42
PS[d]	140			
PEE−PEO	33	0.25	66.2	0.44
PEE[d]	200			
PEP−PEO	2 (M_N)	0.25	66.2	0.44
PEP[e]	3.5			

[a] Calculation of the volume fraction of the PEO domains swollen with CNA is based on the assumption that all CNA present is isolated in the PEO block (see text). The effective volume fraction of the PEO swollen with the dye was determined by neglecting any changes in volume upon mixing, assuming that all CNA present was in the PEO domains, and using the reported densities of CNA, PEO, and the second block. [b] Density = 1.545 g/cm^3 (McPhail, A. T. and Sim, G. A. *J. Chem. Soc.* **1965**, 227−236). [c] Density = 1.229 g/cm^3 for the 7_2 helix of PEO (Takahashi, Y. and Tadokoro, H. *Macromolecules* **1973**, *6*, 672−675). [d] Density = 1.053 g/cm^3 for PS, 0.870 g/cm^3 for PEE (Mark, J. E. P*hysical Properties of Polymers Handbook*; AIP Press, Woodbury, New York, 1996). [e] Density = 0.854 g/cm^3 for PEP (Bates, F. S.; et al. *Macromolecules* **1992**, *25*, 5547−5550).

Indeed, independent infrared measurements of CNA dispersed in the nonpolar homopolymers indicated negligible solubility in PEE and PEP and low solubility in PS. This establishes that at and below 66.2 wt % CNA (relative to PEO), the host−guest diblock composites can be described as having complex α in the PEO domains surrounded by the matrix of the second block. This is corroborated by wide-angle X-ray diffraction peaks that were identical to those observed for the PEO-CNA complex α in pure PEO (Figure 6). Reflections from pure CNA or PEO were not observed at 66.2 wt % CNA, indicating that all the CNA and PEO was consumed in complex formation.

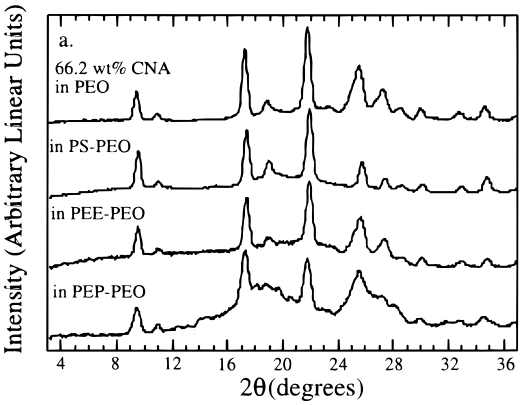

Figure 6. (a) Wide-angle X-ray diffraction data for the PEO: CNA complex α in three diblock copolymers, obtained for samples in which the concentration of CNA was 66.2 wt % with respect to the PEO block. The PEO-CNA molecular complex forms in the PEO block of all three diblock copolymers.

Microstructure of Copolymer−CNA Mixtures. The preferential segregation of CNA to the PEO block effectively adds to the volume fraction of these domains, suggesting probable changes in the microstructure of the copolymer. The volume fraction of PEO in the pure copolymers is 0.22 or 0.25 (Table 1), values which typically give rise to hexagonally packed cylinders of PEO within a matrix of the second block.[43] Indeed, room-temperature small-angle X-ray scattering data for the PEP−PEO copolymer used here were consistent with a cylindrical microstructure having an intercylinder spacing of 87 Å (Figure 7, Table 2).

Unfortunately, the number of reflections from the other two copolymers was insufficient to allow a definitive assignment of microstructure. The ratios of the scattering vectors of the two reflections from PS-PEO are characteristic of either a spherical or cylindrical phase and only one reflection was observed for PEE-PEO.

The scattering data for samples containing 10 wt % CNA with respect to PEO were somewhat more definitive, owing to the improved scattering contrast provided by CNA. The effective volume fraction of the PEO swollen with 10 wt % CNA increases only to 0.26 for all three copolymers. Neglecting changes in entropy and the segment−segment interaction parameter χ caused by the addition of CNA, the hexagonal cylindrical microstructure of the lower CNA concentrations is expected to persist for these new values.[43] Indeed, SAXS data acquired for these at room temperature were characteristic of a cylindrical microstructure. Although assignment of the microstructure of 10 wt % CNA in

(43) Schultz, M. F.; Bates, F. S. In *Physical Properties of Polymers Handbook*; Mark, J. E., Ed.; AIP Press: Woodbury, New York, 1996; pp 427−433.

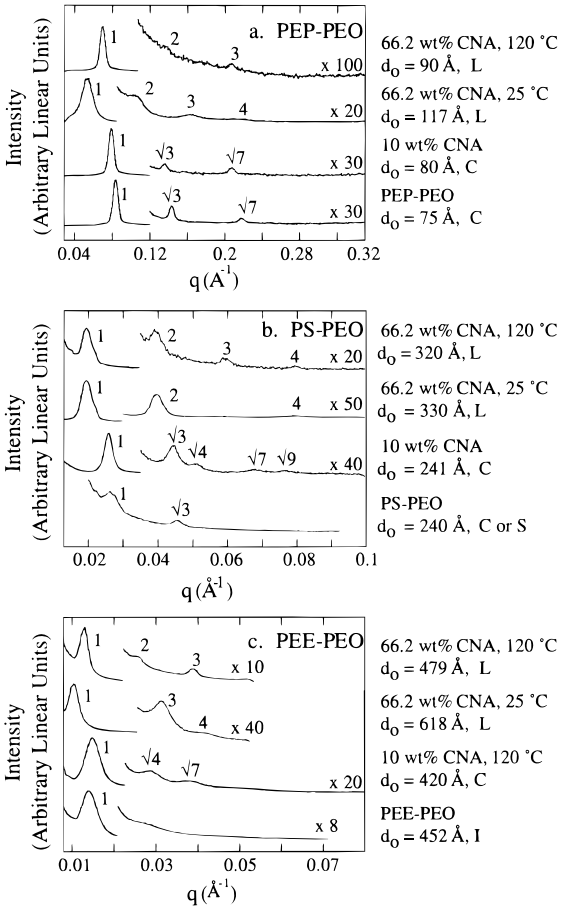

Figure 7. Small-angle X-ray diffraction data for CNA in (a) PEP−PEO, (b) PS-PEO, and (c) PEE-PEO. Concentrations of CNA are given with respect to the PEO block. Data were collected at 25 °C unless otherwise specified. d_o is the characteristic spacing of the reflection corresponding to the lowest scattering vector. The scattering vector for each reflection is normalized to the position of the first, most intense reflection. The pattern of these normalized values was used to identify the phase, or phases, present, which are indicated by L for lamellae, C for hexagonal cylinders, S for spheres, and I for inconclusive.

Scheme 2

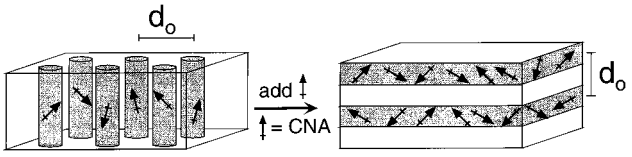

PEE-PEO was not possible at 25 °C because of an insufficient number of well-resolved reflections, the data clearly indicated the presence of hexagonal cylinders when the sample was at 70, 90, or 120 °C.

SAXS data acquired for diblock samples containing 66.2 wt % CNA with respect to PEO (the composition of α) indicated a lamellar microstructure between room temperature and 120 °C (Figure 7, Scheme 2), the latter exceeding the melting points of pure PEO (63 °C), CNA (111 °C), and the molecular complex (82 °C). This indicates that the lamellar microstructure exhibited by all three diblock copolymers containing CNA at this concentration is associated with selective partitioning of CNA to the PEO domain (Table 1) and is not simply a consequence of crystallization of α in the PEO domains.

Lamellae are typically formed when the volume fraction of one block is between 0.4 and 0.6, a range that includes the effective volume fraction $f_{(PEO+CNA)} = 0.46$ at 66.2 wt % CNA. However, we note that the conformational asymmetry of PEE and PEO affords a phase diagram that is asymmetric about $f = 0.5$ and a gyroid phase at $f_{(PEO)} = 0.46$.[44] The observation of a lamellar phase at fraction $f_{(PEO+CNA)} = 0.46$ illustrates that precise prediction of the microstructure of copolymer−CNA composites directly from the phase diagram of the pure copolymers is tentative. This discrepancy can be attributed to changes in the relative free energies upon introduction of additives, as suggested by calculations for A/A−B blends.[45] Calculation of an effective volume fraction in the manner used here assumes that the addition of the chromophore has the same thermodynamic effect as changing the relative volume fractions of the two blocks. However, the conformational change of PEO due to formation of the complex α can introduce changes in the tension of the diblock interface that are not anticipated by assuming that CNA behaves as PEO.

Transformations of microstructure upon selective incorporation of water by the PEO domain of PEE-PEO[44] and a temperature-driven change of guest partitioning between two domains of polystyrene-poly(4-vinylpyridine) have been reported.[19b] Similarly, the segregation of a sol−gel within PEO domains of block copolymers yields an inorganic−organic composite with a templated microstructure that, depending on the concentration of the sol−gel, can differ from the morphology of the pure copolymer.[10] We note that changes in χ have been suggested to influence the microstructures of blends comprising PEP−PEO and an epoxy selectively solvated by PEO.[46] Although the changes in morphology observed upon CNA inclusion can be influenced by χ (i.e., $\chi_{PEE-PEO}$ will differ from $\chi_{PEE-PEO:CNA}$), we surmise that the behavior here is dominated by the increase in $f_{(PEO)}$ upon CNA inclusion.

The separation between the PEO domains increases with CNA concentration (Table 2), this separation varying with temperature. In the case of the lamellar microstructure of the samples containing 66.2 wt % CNA, the characteristic spacing of the lamellae (d_o) is larger at 25 °C than at 120 °C. This can be attributed to chain folding in the crystalline PEO domain at the lower temperature that is absent above the melting point. Similar behavior has been noted for PE-PEE copolymers.[47] Of the three materials considered here, the PS-PEO:CNA composite undergoes the smallest change in d_o upon crystallization. This suggests that conformational changes in the PEO domains required for changes in lamellar spacing are frustrated by the glassy PS block ($T_g = 89$ °C). In contrast, the significantly lower glass transition temperatures of PEE and PEP (<0 °C) allow for more facile conformational changes during crystallization of the PEO domains and the accompanying expansion of the interlamellar spacing.

(44) Hajduk, D. A.; Kossuth, M. B.; Hillmyer, M. A.; Bates, F. S. *J. Phys. Chem. B* **1998**, *102*, 4269−4276.
(45) Matsen, M. W. *Macromolecules* **1995**, *28*, 5765−5773.
(46) Lipic, P.; Bates, F. S.; Hillmyer, M. A. *J. Am. Chem. Soc.* **1998**, *120*, 8963−8970.
(47) Ryan, A. J.; Hamley, I. W.; Bras, W.; Bates, F. S. *Macromolecules* **1995**, *28*, 3860−3868.

Table 2. Summary of Small Angle X-ray Scattering Results for the Composites of CNA in PS-PEO, PEE−PEO, and PEP−PEO at Selected Concentrations of CNA (with respect to PEO)

	wt% CNA relative to PEO			
	0	10	66.2, 25 °C	66.2, 120 °C
PS-PEO				
microstructure	cylindrical (or spherical)[b]	cylindrical	lamellar	lamellar
d_o (Å)	240	241	330	320
distance between PEO domains (Å)[a]	277	278	330	320
PEE-PEO				
microstructure	inconclusive[c]	cylindrical (120 °C)[d]	lamellar	lamellar
d_o (Å)	452	458 (25 °C)[d]	618	479
distance between PEO domains (Å)[a]	523	529 (25 °C)[d]	618	479
PEP-PEO				
microstructure	cylindrical	cylindrical	lamellar	lamellar
d_o (Å)	75	80	117	90
distance between PEO domains (Å)[a]	87	92	117	90

[a] Values for samples containing 0 and 10 wt % CNA relative to PEO were calculated from d_o, assuming the PEO domains are hexagonally packed and $a = (2/\sqrt{3})d_o$. [b] Only two reflections were observed so that the microstructure cannot be definitively assigned. The volume fraction of PEO ($f = 0.25$) and the reflections observed for the 10 wt % sample suggest that the pure copolymer has a cylindrical microstructure. [c] Only one reflection was observed. [d] The number of reflections was sufficient to allow assignment of the microstructure only when the sample was at 70, 90, or 120 °C. The scattering vector of the sole strong reflection from the sample at 25 °C was used to calculate a distance between the PEO domains, assuming these domains to be hexagonally packed cylinders. The data for this sample was collected at 120 °C.

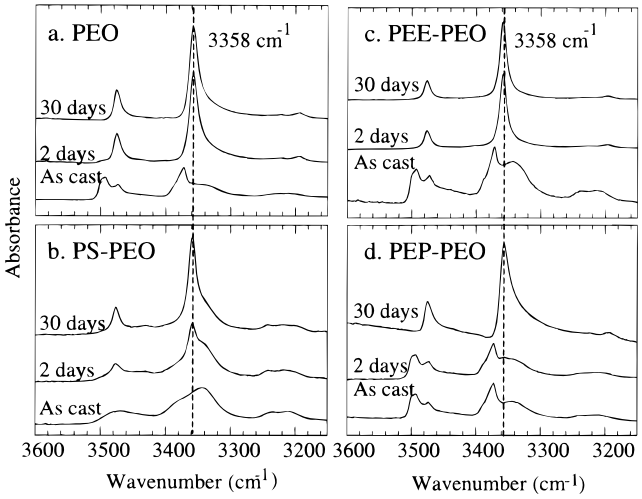

Figure 8. Infrared spectroscopic data for spin-cast thin films of CNA in (a) PEO, (b) PS-PEO, (c) PEE-PEO, and (d) PEP−PEO acquired at different times following preparation. The composition of each sample was 66.2 wt % CNA relative to the PEO domain. The position of the band unique to the PEO-CNA molecular complex, 3358 cm^{-1}, is indicated for reference.

Phase Behavior of CNA in the Diblock Copolymers. Phase diagrams were constructed from DSC and FTIR spectroscopy measurements, the latter relying on analysis of the asymmetric and symmetric stretching modes of NH_2 (Figure 8, Table 3). The phase diagram obtained for PS-PEO:CNA mixtures (Figure 9) strongly resembles that observed for CNA in PEO, exhibiting a eutectic point and the compositionally invariant line for the molecular complex α. However, in the diblock composite the compositions at which these features appear shift to higher concentrations of CNA, from 25% to 43% and 66.2% to 70%, respectively. This can be attributed to the slight solubility of CNA in polystyrene, which is revealed by the infrared spectra of PS-PEO:CNA blends (a weak band at 3400 cm^{-1}) having chromophore concentrations less than 66 wt %.

Although the phase diagrams were determined using samples that had been aged for at least 30 days so that equilibrium was more likely, precise determination of the phase regions is probably complicated by the slow kinetics observed for the formation of α in the diblock composites. Furthermore, infrared spectroscopy revealed bands that could not be assigned to α. These bands were attributed to other complexes with structures slightly different than α, possibly configurations that exist at the PS/PEO interface where the PEO chains cannot adopt the zigzag conformation required for α.

Table 3. FTIR Data for CNA−Diblock Copolymer Composites

phase label	NH_2 ν_{as} and ν_s (cm^{-1})	NH_2 β_s (cm^{-1})	description of phase
α	3475; 3358	1615	1:2 CNA:EO molecular complex
β	3466; 3343; broad	1626	CNA dissolved in PEO
γ	3399	*a*	CNA dissolved in PS
δ	3388	1631	CNA phase-separated in PS
CNA (s)	3494, 3474; 3374	1625	solid, phase-separated CNA
CNA (l)	3484; 3380; broad	1623	molten, phase-separated CNA

[a] No βs band characteristic of CNA dissolved in PS was present. The band observed at 1615 cm^{-1} was instead assigned to the PEO:CNA molecular complex, which was simultaneously present in the other block of the copolymer.

The CNA chromophore is less soluble in PEE and PEP than in PS. This difference in solubility is manifest in the corresponding PEO-based diblocks. The PEE-PEO and PEP-PEO systems are sufficiently similar that their behavior can be adequately represented by PEE-PEO alone. Infrared bands characteristic of bulk CNA appear in PEE homopolymer at CNA concentrations exceeding 4 wt % (Figure 9c). Spectra of CNA in PEE-PEO revealed no signature of CNA *dissolved* in PEE, as surmised from the absence of infrared bands similar to those observed for CNA dissolved in hexane.

A feature that distinguishes the PEE-PEO:CNA system from its PS-PEO counterpart is the occurrence of an endotherm, corresponding to the melting of crystalline dye (110 °C), at all compositions. This feature, and the occurrence of endotherms for the transitions associated with α and PEO at all composi-

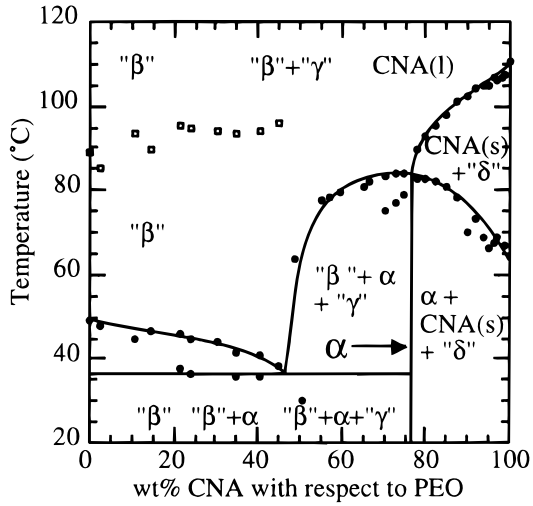

Figure 9. Phase diagram for CNA in PS-PEO. The CNA concentration is relative to PEO. CNA and the CNA-containing phases α, *β*, *δ*, and *γ* indicated on the phase diagrams were detected in the infrared spectroscopic data. The latter three, in quotes, were not evident from X-ray data and the endotherm determinations did not produce distinct regions corresponding to these phases, presumably because kinetic limitations hamper achievement of thermodynamic equilibirum. The endotherm data points are depicted on the diagrams and the phase regions were constructed by interpolation. The glass transitions of the PS block are denoted as filled circles and open squares, respectively.

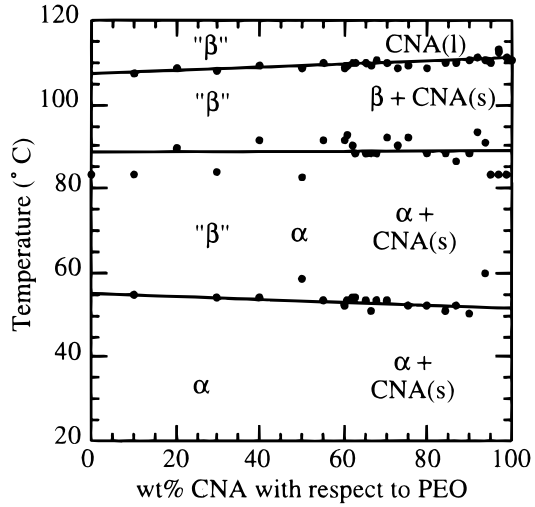

Figure 10. Phase diagram for CNA in PEE−PEO. The CNA concentration is relative to PEO. The CNA-containing phases α and *β* indicated on the phase diagrams were identified from infrared spectroscopic data. The *β* phase is included in quotes because it was not observed in X-ray data. The phase regions indicated are not thermodynamically valid. However, the endotherm determinations did not reveal distinct regions corresponding to these phases, presumably because kinetic limitations hamper achievement of thermodynamic equilibrium.

tions, produces a phase diagram for PEE-PEO:CNA that differs substantially from that of PS-PEO:CAN (Figure 10). This behavior suggests substantial kinetic barriers to the achievement of thermodynamic equilibrium on the time scale of sample preparation. For example, the endotherm identified as melting of pure CNA can be attributed to bulk CNA that formed from immiscible CNA that pooled as a phase-separated liquid in PEE at the temperature (120 °C) used to process the samples prior to quenching to room temperature. The negligible solubility of CNA in PEE would inhibit diffusion of molecular CNA into the PEO domain. Consequently, even at low concentrations of chromophore, metastable CNA crystallites are trapped in the PEE domains of the room-temperature samples used for DSC analysis.

In contrast, the calorimetric traces of the PS-PEO: CNA system exhibited endotherms attributable to melting of the phase-separated crystalline CNA only when the concentration of the CNA was greater than 75 wt % with respect to PEO. If the concentration was below this threshold, after cooling from the melt some CNA remained as a nonbulk phase in the PS matrix because CNA was dispersed as a soluble component in PS at 120 °C. After quenching to room temperature, diffusion of CNA molecules within PS, required for crystallization of bulk CNA in PS, would be limited by the glassy nature of this block.

Nevertheless, the data suggest that the PS block acts as a solvent (albeit a relatively poor one) that is capable of transporting CNA to adjacent PEO lamellae at the elevated temperatures, thereby permitting that formation of the thermodynamically preferred α. In contrast, the PEE and PEP blocks serve as a barrier by trapping phase-separated liquid CNA at the elevated temperatures such that equilibrium cannot be achieved on the time scale of sample processing. This effect is probably exacerbated by the lamellar microstructure adopted by these compositions. This argues that the design of diblock:chromophore composites should include a second block that not only reinforces the microstructure and provides desirable mechanical properties, but is also capable of dissolving small amounts of the chromophore so that it can be delivered to the companion block that complexes the chromophore. We note that similar effects of crystallization conditions on morphology and phase behavior have been reported for other polymeric systems.[48]

Endotherms in data for CNA in PEE-PEO were also observed at the temperatures corresponding to the melting of the molecular complex (82 °C) and the eutectic transition (54 °C) for all CNA compositions. These endotherms are not order-to-disorder transitions (ODT) of the copolymer; rheological experiments reveal that the ODT's of both PS-PEO and PEE-PEO are thermally inaccessible (>250 °C). The observation contrasts with behavior for CNA in either PS-PEO or PEO homopolymer. Although the reasons for these differences between the phase diagrams are presently unclear, the data suggest significant departures from thermodynamic equilibrium. We note that thermal transitions of complexes involving PEO and NaSCN or KSCN were only observed for the first heating cycle or were reversible only for slow rates of cooling.[27,49]

The complications posed by the lack of thermodynamic control for the diblock:CNA composites are further illustrated by discrepancies between the DSC and FTIR data. For example, DSC indicates three endotherms for 40 wt % CNA in PEE-PEO, whereas FTIR reveals only the melting of α between 70 and 90 °C. This may be due to the slower heating rates (1 °C/

(48) Li, Y.; Jungnickel, B.-J. *Polymer* **1993**, *34*, 9−15.
(49) Robitaille, C.; et al. *Macromolecules* **1987**, *20*, 3023.

min vs 5 °C/min for DSC) as well as the thin film character of the composites (2 μm thick) used for the FTIR studies.

The spin-coated samples were not at equilibrium immediately after preparation; their FTIR spectra in PEO and all the copolymers evolved over days at room temperature (Figure 8). During this time, bands characteristic of $\nu(NH_2)$ for the complex (3474 and 3358 cm^{-1}) appeared at the expense of bands characteristic of any phase-separated CNA (3494, 3474, and 3374 cm^{-1}) or CNA dissolved in PEO (3343 cm^{-1}, broad). The band at 3358 cm^{-1} generally appeared within 1 week of sample preparation, although the rate of complex formation was highly variable and not reproducible.

Conclusion

The phase behavior of CNA in PEO homopolymer and PS-PEO, PEE-PEO, and PEP−PEO diblock copolymers reveals that CNA preferentially segregates to the PEO domain accompanied by the formation of a crystalline molecular complex with triclinic symmetry. The combination of wide-angle X-ray diffraction and infrared spectroscopy enable construction of a structural model in which the PEO chains adopt a nominally all-trans zigzag configuration, the chains organized as (100) layers separated by layers of one-dimensional stacks of CNA molecules. Polarized infrared measurements indicate that the molecular planes of the CNA molecules are nominally perpendicular to the PEO chains. The metrics associated with the zigzag PEO configuration appear to allow for optimal hydrogen bonding between the PEO oxygen atoms and the amine protons of the CNA chromophores as well as hydrogen bonding between CNA molecules in adjacent stacks.

The conformational rigidity associated with a crystalline complex such as the one identified here offers considerable advantages for the design of SHG materials as entropically driven disordering will be inhibited compared to noncrystalline polymer−chromophore materials. The results described here suggest that the presence of a second block somewhat hinders the formation of the crystalline PEO:CNA complex and induces the formation of complexes with slightly different structures. The second block also appears to play an important role with respect to the ability of the composite to achieve equilibrium. The design of diblock: chromophore composites should rely on a second block that not only serves the reinforce the microstructure and provide desirable mechanical properties, but also is capable of dissolving the chromophore so that it does not phase separate in the melt and can be delivered to the companion block that complexes the chromophore.

Whereas wide-angle X-ray diffraction provides elucidation of the structure of the PEO:CNA complex, small-angle X-ray diffraction reveals that the segregation of CNA to the PEO domains alters the diblock copolymer microstructure from the hexagonal cylinder phase to the lamellar phase at the composition of the complex. This demonstrates that the design of such materials requires attention to the influence of the chromophore on the polymer microstructure as well as the ordering at the molecular level. Nevertheless, the formation of a rigid crystalline complex in a well-defined polymer microstructure suggests substantial opportunities for permanent macroscopic noncentrosymmetric ordering of chromophores. The mechanical robustness of such materials also makes them more amenable to thin-film and bulk processing compared to the bulk chromophores alone.

Although the chromophore concentration is reduced in the polymer films compared to the pure bulk form, the materials described here contain such large amounts of CNA (nearly 67% in PEO) that the effect of dilution on nonlinear optical response should be minimal. Furthermore, the chromophore orientation with respect to the macroscopic plane of thin films of these composites may be adjustable through anisotropic electric field poling as the films are cooled from the melt. We anticipate that this approach to controlling hierarchical structure over length scales spanning several orders of magnitude will lead to new optoelectronic materials.

Experimental Section

Materials and Methods. 2-Chloro-4-nitroaniline (Aldrich, 99%) was recrystallized twice from toluene and ethanol (2/1 v/v) and dried under vacuum. The PEO used for calorimetric measurements and for casting supported films from solution had a molecular weight of 8000 g/mol (Aldrich). The M_w of deuterated PEO used in control studies was 43 300 g/mol (Polymer Source, Inc.). Composite films were prepared by casting CNA and PEO (40 g/L) from a common solvent, acetonitrile (EM Science, HPLC grade, 99.99%), onto several substrates. Round glass coverslips and NaCl disks were spin coated, whereas polyethylene substrates were coated by static casting of the solutions. The spin-coated films were 1−3 μm thick, as determined by profilometry. PEO with a molecular weight of 5×10^6 g/mol (Polysciences, Inc.) was used to prepare free-standing films crystallized from melt. Poly(styrene) (PS) was prepared by anionic polymerization, whereas poly(ethylethylene) (PEE) and poly(ethylpropylene) (PEP) were prepared by anionic polymerization followed by catalytic hydrogenation. PS-PEO, PEE-PEO, and PEP-PEO were prepared by anionic polymerization using published procedures.[50] PEE-PEO was purified of ionic impurities by dissolving the polymer in chloroform and repeatedly washing with deionized water. The chloroform was evaporated, and the residue was dried at 70 °C under vacuum. After purification, the amounts of potassium and lithium remaining were less than 32 and 6 ppm, respectively (Galbraith Labs, Knoxville, TN).

Differential Scanning Calorimetry. Each sample for differential scanning calorimetry (DSC) was prepared by adding 10−15 mg of a mixture containing the desired amounts of CNA and PEO to a stainless steel, high volume pan. Samples were melted and allowed to recrystallize at least three times before data for the phase diagram were acquired. The calorimetric traces were recorded using a Perkin-Elmer Pyris 1 DSC programmed to heat at 5 °C/min (indium reference). Standard solutions of the three diblock copolymers and PS, PEE, and PEP were at a concentration of 40 g/L in tetrahydrofuran (EM Science, spectroscopic grade, 99.94%). These solutions were then added to CNA to the desired PEO:CNA ratio. CNA concentrations in diblock copolymers are denoted in the text as weight percentages of CNA *measured relative to the PEO block*. For the purpose of sample preparation, the corresponding concentration of CNA with respect to an entire copolymer of a given molecular weight was determined by converting the volume fraction of PEO in the pure diblock copolymer to a weight fraction.

FTIR Spectroscopy. Infrared spectra in the region 4000−500 cm^{-1} were recorded with 2 cm^{-1} resolution on a Nicolet Magna 550 FTIR equipped with a DTGS detector. Depending on the signal-to-noise ratio, either 64 or 128 interferograms were summed to produce each spectrum. Samples were thin

(50) Hillmyer, M. A.; Bates, F. S. *Macromolecules* **1996**, *29*, 6994−7002.

films cast onto NaCl disks (vide ante). Sodium and other alkali metal ions form complexes with PEO;[51] therefore, films were also prepared on polyethylene and on glass disks to verify the absence of ion complexation. The molecular complex of CNA and PEO exhibited bands at 3475 and 3358 cm^{-1} regardless of the substrate and regardless of storage conditions. Spectra of pure CNA was acquired neat in Nujol mulls, as 20 mM solutions in toluene (EM Science, spectroscopic grade, 99.98%), ethylene glycol dimethyl ether (monoglyme) (Aldrich, 99%), and hexane (Mallinckrodt, spectroscopic grade). Solutions were contained in a liquid cell fitted with KBr windows. The spectrum of the solvent was subtracted before the data was analyzed. Far-infrared spectra (700−100 cm^{-1}) of free-standing, uniaxially aligned films or CNA dispersed in polyethylene were acquired from 256 summed interferograms recorded with 2 cm^{-1} resolution on a Nicolet Magna 760 IR. Polarized spectra were recorded for uniaxially aligned, free-standing films of the molecular complex, oriented with the fiber axis vertical. With the sample position constant, FTIR spectra were recorded using light polarized parallel or perpendicular to the fiber axis. The dichroic ratio was calculated from the absorbances of each vibrational band ($R = A_{\parallel}/A_{\perp}$). Bands with parallel polarization have $R > 1$, while bands with perpendicular polarization have $R < 1$.

Spectra of the diblock copolymer films containing CNA were recorded periodically to monitor any changes. Complex formation with PEO generally occurred within 1 week of sample preparation, but this rate was highly variable and not reproducible. Infrared spectra of CNA in the diblock copolymer films (Figure 9) were recorded 30 days after the films were prepared. No significant changes had occurred in the positions or intensities of the bands for at least 15 days prior to the collection of the data. Polymer films that were monitored spectroscopically while in a heated cell had aged at room temperature for at least eight months prior to data collection. Each film cast on NaCl was covered with another disk of NaCl and then heated from room temperature to 130 °C at 1 °C/min. This relatively slow heating rate was required for an adequate signal-to-noise ratio and automated collection of spectroscopic data, which was initiated as the sample reached previously established set point temperatures. Similar experiments with pure CNA were performed with CNA that had been spin cast from methanol onto a NaCl disk.

Wide-Angle X-ray Diffraction. Fiber patterns of the complex α and powder patterns of the polymers and polymer-CNA composites were obtained with a Bruker microdiffractometer equipped with a Cu Kα source, a nickel filter, and a moveable 2D area detector. The source was operated at a voltage and tube current of 45 kV and 40 mA, respectively. The sample, a free-standing film, was initially mounted on the four-circle goniometer head with the draw axis vertical and the plane of the film perpendicular to the incident beam. A series of frames was then recorded, each corresponding to a unique setting of angles 2θ, ω, χ, and ϕ (Supporting Information). This method of data collection in multiple frames with a long sample-to-detector distance allowed optimization of both the number and resolution of reflections, which were recorded through a maximum 2θ angle of at least 65°. The sample-to-detector distance, 15.1 cm, was verified following data collection by painting the fiber with a silver lacquer reference and recollecting selected sets of reflections. To eliminate and to verify the diffraction peaks associated with uncomplexed crystalline PEO, some samples of α were also prepared for X-ray diffraction by soaking uniaxially aligned films of PEO for at least 20 h in ether saturated with CNA. The density of the complex was measured by flotation of melt-processed blends in mixtures of heptane and carbon tetrachloride.

Reciprocal lattice parameters a^*, b^*, and γ^* were determined from the equatorial reflections ($l = 0$) by finding a self-consistent set of indices for ($hk0$) which minimized the errors in the quantity $d_{\text{observed}}{}^{*2} - (h^2a^{*2} + k^2b^{*2} + 2hka^*b^* \cos \gamma^*)$. By trial and error, all remaining nonmeridional and nonequatorial reflections were then assigned a self-consistent set of indices which minimized the errors in $d_{\text{observed}}{}^{*2} - (h^2a^{*2} + k^2b^{*2} + l^2c^{*2} + 2klb^*c^* \cos \alpha^* + 2lhc^*a^* \cos \beta^* + 2hka^*b^* \cos \gamma^*)$. Details are provided in the Supporting Information.

Uniaxially aligned samples of the complex α for X-ray diffraction were prepared by pressing films ∼110 μm thick between brass or aluminum foils in a Wabash press at 120 °C. The molten blends were quenched in liquid nitrogen i to slow crystallization prior to stretching. The amorphous samples were then removed from the foils and stretched with a draw ratio of at least 4/1 as they warmed to room temperature and crystallized. Unstretched films of both the pure copolymers and the copolymers doped with CNA were prepared with the same initial steps. However, uniaxially aligned films of CNA in the copolymers could not be prepared by drawing because the samples were either too brittle (PS-PEO) or too soft (PEP-PEO, PEE-PEO). Consequently, the diblock copolymer samples were isotropic in the plane of the films. The PS-PEO and PEE-PEO could be handled as free-standing sheets at room temperature, while samples of the lower molecular weight PEP-PEO could not be maintained as films once they had been removed from liquid nitrogen.

The one-dimensional powder diffraction pattern of CNA was recorded with a Siemens D-500 instrument equipped with a Cu Kα source, nickel filter, and a graphite monochromator. Data were recorded over a range $3° \leq 2\theta \leq 70°$ with a step size of 0.05° and dwell time of 38 s. Nickel powder was used as an internal standard.

Small-Angle X-ray Scattering. Small-angle X-ray scattering (SAXS) experiments were performed on an instrument constructed at the University of Minnesota. Nickel-filtered, Cu Kα X-rays were generated by a Rigaku RU-200BVH rotating anode equipped with a 0.2 × 2 mm microfocus cathode and Franks mirror optics. The accelerating voltage and tube current were 41 kV and 60 mA, respectively. A specimen that had been annealed at 120 °C and quenched in a manner identical to that used for the wide-angle diffraction measurements was mounted between two pieces of Mylar. If necessary, thin pieces of isotropic films were stacked to make a sample that was ∼0.5−1 mm thick. The sample was then placed inside an evacuated chamber and maintained at a given temperature (±0.1 °C) with a pair of heaters mounted on a water-cooled brass block. The distance from the sample to the multiwire area detector (HI-STAR, Siemens Analytical X-ray Instruments) was 50 cm for CNA blends with PEP-PEO and PEP-PEO and 2.25 m for all other materials. Data were collected at 25, 50, 70, 90, 120, and again at 25 °C. As the temperature was increased, the copolymer or blend was annealed at each set point for at least 5 min prior to the beginning of data collection. After cooling, the sample was annealed at 25 °C for 30 min before the final data set was collected. Exposure times varied from 1 to 11.5 h, depending on the signal-to-noise ratio.

Each two-dimensional diffraction pattern was corrected for detector response characteristics and converted to a one-dimensional format by azimuthal integration. The phase or possible phases present were identified from the sequence of the scattering vectors after they had been normalized to the position of the first scattering vector, q_0. Lamellae are characterized by peaks at spacings of 1/2/3/4, etc. Usually, the allowed reflections from hexagonal cylinders occur with spacing ratios $1/\sqrt{3}/\sqrt{4}/\sqrt{7}/\sqrt{9}$, etc. For compositions near $f = 0.25$, however, the form factor for the reflection having $q = \sqrt{4}q_0$ is at a minimum.[52] Scattering from a material with a spherical microstructure generally gives peaks at spacings of $1/\sqrt{2}/\sqrt{3}/\sqrt{4}/\sqrt{5}$, etc.

Dynamic Mechanical Spectroscopy. Dynamic elastic and loss shear moduli, G' and G'', respectively, were obtained using a Rheometric Scientific Ares strain-controlled rheometer

(51) (a) Wright, P. V. *J. Mater. Chem.* **1995**, *5*, 1275−1283. (b) Lascaud, S.; Perrier, M.; Vallée, A.; Besner, S.; Prud'homme, J.; Armand, M. *Macromolecules* **1994**, *27*, 7469−7477. (c) Lightfoot, P.; Mehta, M. A.; Bruce, P. G. *Science* **1993**, *262*, 883−885. (d) Chatani, T.; Okamura, S. *Polymer* **1987**, *28*, 1815−1819.

(52) Koppi, K. A.; Tirrell, M.; Bates, F. S.; Almdal, K.; Mortensen, K. *J. Rheol.* **1994**, *38*, 999−1027.

Table 4. Infrared Spectroscopic Data for the Vibrational Modes of CNA, PEO, and the Molecular Complex of CNA with PEO[a]

CNA in Nujol	PEO uniaxial fiber		complex in PEO-d_4 on PE	complex in PEO on PE[b]		assignment[c,d]	symmetry
3494						ν_{as} NH_2	a′ (ip)
3474			3476	3476	⊥	ν_{as} NH_2	a′ (ip)
			3430	3431	⊥	ν NH_2	
3374						ν_s NH_2	a′ (ip)
			3358	3358	⊥	ν_s NH_2	a′ (ip)
	2947	⊥		2943		ν_{as} CH_2	
			2918	2914	⊥		
	2886	∥, ⊥					
				2873	⊥		
1628						β_s NH_2	a′ (ip)
			1617	1617	⊥	β_s NH_2	a′ (ip)
1589			1588	1588	⊥	8b ring vibration	a′ (ip)
1580			1580	1579		ν C−C	a′ (ip)
			1559				
			1539	1539	∥		
			1500	1504	⊥	$\delta(CH_2)$ planar zigzag PEO	
1486			1492	1488		ν_{as} NO_2	a′ (ip)
	1467	⊥				$\delta(CH_2)a-\delta(CH_2)_s$	E_1
	1463	∥				$\delta(CH_2)_a$	A_2
	1456	∥				$\delta(CH_2)_a$	A_2
	1452	∥				β_s CH_2	
			1426	1426	⊥		
	1413	⊥				$\omega(CH_2)_a$	E_1
				1385			
	1361	⊥				$\omega(CH_2)_s+\nu(CC)$	E_1
	1350	∥					
	1346	∥				$\omega(CH_2)_a$	A_2
			1337	1337		$\omega(CH_2)$ planar zigzag PEO	
	1325	∥					
			1319	1319		ν (C−N)	
1309						ν (C−N)	a′ (ip)
	1288	⊥					
	1282	⊥				CH_2 twisting	
			1279	1278	⊥	β C−H bend ip	a′ (ip)
1262						β C−H bend ip	a′ (ip)
			1254	1254	⊥	β C−H bend ip	a′ (ip)
	1242	∥				$\tau(CH_2)_a$	A_2
	1235					$\tau(CH_2)_s-\tau(CH_2)_a$	E_1
				1231	⊥	$\tau(CH_2)$	
			sh	1140			
1127	1126		1128	1127	∥, ⊥	ν(COC) for PEO; $\delta(CD_2)_s + \nu(COC)_s$ for PEO-d_4; β(C−H) 18a (CNA)	
			1091			$\delta(CD_2)_a$; $\delta(CD_2)a - \delta(CD_2)_s - \omega(CD_2)_a$	
	1061	⊥				$\nu(COC)_a + r(CH_2)_s$	E_1
			1048	1047	⊥		
1033						β_{as} NH_2	a′
			1015	1014	⊥	$r(CH_2)_a + \nu(COC)$ of *trans* $O-(CH_2)_2-O$	
			996			$\tau(CD_2)_a$	
	958	∥		959	⊥	$r(CH_2)_a$	A_2 (PEO)
	947	⊥				$r(CH_2)_s - \nu(COC)_a$	E_1
			941			$\tau(CD_2)_a + \tau(CD_2)_s$; $\nu(COC)_a+\omega(CD_2)_a - \tau(CD_2)_a$	
			897	897	⊥	β_s NO_2	a′ (ip)
893						β_s NO_2	a′ (ip)
			887	887	∥		
	877		878				
	844	⊥				$r(CH_2)_a$	E_1
			837	837	∥	$r(CH_2) - \tau(CH_2)$ planar zigzag PEO	
824					∥	β C−H	a″ (op)
			821	821	⊥	ν C−C	a′ (ip)
817						ν C−C	a′ (ip)
746			746	746	∥	γ_s NO_2	a″
722						ν C−Cl	a′ (ip)
705							
668			668				
641			641	641	⊥	α (CCC)	a′ (ip)
	580	∥					
				562	⊥, ∥	$\delta(COC) - \delta(CCO)$ planar zigzag PEO	
550			550	550	⊥	β_{as} NO_2	a′ (ip)
532	533	⊥	533	532	∥	16b (a″, CNA); $\delta(OCC)_a - \delta(COC) - \nu(COC)_s$	a″; E_1
	529	∥				$\delta(OCC)_a$	A_2
	510	∥				$\delta(OCC)_a$	A_2
			491				
				484	⊥		

Table 4 (Continued)

CNA in Nujol	PEO uniaxial fiber		complex in PEO-d_4 on PE	complex in PEO on PE[b]		assignment[c,d]	symmetry
				457			
			452			$\delta(OCC)_a - r(CD_2)_a$	
			441				
434			434			ring vibration	a′ (ip)
			425				
			380	380	⊥		
362			364	364	⊥	α(CCC)	a′ (ip)
309							
			291	290		δ(CCO) of planar zigzag PEO	
			282	282	⊥		
274							
	216	⊥				$\delta(OCC)_s - \delta(COC) - \delta(OCC)_a - \tau(CC)$	E_1
190			191		∥		
				188	⊥		
			167				
	164	⊥				$\tau(CC) + \tau(COC)_a$	E_1
	105	∥				$\tau(COC)_a$	A_2

[a] Band locations are given in cm^{-1}. The polarization of the bands was determined using uniaxially aligned fibers of PEO or of the complex in PEO and is indicated to the right of the frequency. [b] Polarization data were from spectra of uniaxially aligned fibers. Band locations were determined from spectra of isotropic thin films, which provided better resolution of the vibrational bands than did uniaxially aligned fibers. [c] References for band assignments: (*i*) Nazar, L. F.; Wu, H.; and Power, W. P. *J. Mater. Chem.* **1995**, *5*, 1985−1993. (*ii*) Da Costa, V. M.; Fiske, T. G.; and Coleman, L. B. *J. Chem. Phys.* **1994**, *101*, 2746−2751. (*iii*) Reddy, V. B.; Rao, G. R. *Vibr. Spectrosc.* **1992**, *4*, 67−75. (*iv*) Papke, B. L.; Ratner, M. A.; and Shriver, D. F. *J. Phys. Chem. Solids* **1981**, *42*, 493. (*v*) Varsanyi, G. *Assignments for Vibrational Spectra of Seven Hundred Benzene Derivatives*; John Wiley & Sons, New York, 1974; Vol. 1. (*vi*) Verma, V. N. *Spectrosc. Lett.* **1973**, *6*, 23−40. (*vii*) Verma, V. N.; and Nair, K. P. R. *Indian J. of Pure Appl. Phys.* **1970**, *8*, 682−683. (*viii*) Matsuura, H.; Miyazawa, T. *Bull. Chem. Soc. Jpn.* **1968**, *41*, 1798−1808. (*ix*) Yoshihara, T.; Tadokoro, T.; Murahashi, S. *J. Chem. Phys.* **1964**, *41*, 2902−2911. [d] Vibrational modes: α, in-plane ring deformation; β, scissoring; δ, bending; ϕ, out-of-plane ring deformation; γ, out-of-plane bending; ν, stretching; τ, twisting; ω, wagging; r, rocking; s, symmetric, a, antisymmetric relative to the 2-fold axis perpendicular to the helix and passing through the center of the C−C bond; + or − indicates the phase relations of coupled coordinates.

with a shear sandwich geometry. Data were examined for signs of order-to-disorder transitions, which are indicated by a large discontinuous decrease in modulus. Samples were heated at 1 °C/min and sheared with 3% strain at a frequency of 1 rad/s.

Acknowledgment. The authors are grateful to Dr. Marc Hillmyer, Paul Lipic, and Chin Chu for synthesizing the diblock copolymers used in these studies, to Dr. Hillmyer and Dr. Pascal Damman for helpful discussions, and to Linda Sauer, Dr. Richard Ortega, and Uwe Preckwinkel for assistance with wide-angle X-ray diffraction. Financial support was provided by the University of Minnesota Center for Interfacial Engineering and by the MRSEC Program of the National Science Foundation under Award Number DMR-9809364.

Supporting Information Available: Table of calculated densities for various EO:CNA compositions, table of calculated vs observed scattering patterns for the uniaxially drawn 2:1 PEO:CAN complex, and temperature-dependent infrared spectra for PE-PEO:CNA and PEE-PEO:CNA thin films. This material is available free of charge via the Internet at http://pubs.acs.org.

CM9905794